

Understanding of electrochemical behaviors of niobium in molten LiCl–KCl eutectic for pyrochemical decontamination process

Gwan Yoon Jeong, Sungjune Sohn, Younghwan Jeon, Jaeyeong Park*

School of Mechanical, Aerospace and Nuclear Engineering, Ulsan National Institute of Science and Technology, 50 UNIST-gil, Ulsju-gun, Ulsan, 44919, Republic of Korea

HIGHLIGHTS

- Electrochemical behaviors of Nb in LiCl–KCl were identified by cyclic voltammetry.
- Apparent potentials for redox reactions of Nb are verified with literature.
- Pyrochemical decontamination processes for Nb-containing wastes are proposed.

ARTICLE INFO

Article history:

Received 27 March 2019
Received in revised form
7 June 2019
Accepted 26 June 2019
Available online 27 June 2019

Keywords:

Niobium
LiCl–KCl
Cyclic voltammetry
Peak potential
X-ray diffractometry

ABSTRACT

In this study, the electrochemical behaviors of niobium were examined with 1.0 wt% of NbCl₅ in the molten LiCl–KCl at 450 °C via different electrochemical techniques. A chronoamperometry was performed to prepare solutions containing the selected oxidation state of the Nb ion, and the color of the solution was compared to the literature data. Cyclic voltammeteries were performed with a combination of different scan ranges and scan rates using an electrochemical cell prepared by LiCl–KCl–NbCl₅ salt mixture and an inert tungsten electrode. Five oxidation and four reduction peaks were found, and possible redox reactions attributing to each peak were identified based on the rate of change of the current density as a function of the scan rate. It was found that Nb(V) can be deposited as a metallic Nb via Nb(IV), Nb(III), and Nb(II), and the deposition of the metallic Nb is perturbed by the formation of insoluble nonstoichiometric Nb chloride compounds on the electrode surface. Three irreversible oxidation peaks were caused by the oxidation of metallic Nb and insoluble Nb chlorides, which competed with each other, but the dissolution of metallic Nb became dominant as the scan rate increased. X-ray diffraction analysis was performed to examine the possibility of a chemical reduction of Nb(V) to Nb(IV), but no evidence was found, which indicated the initial concentration of Nb(V) was preserved in all the experiments. It was also found that the different pyrochemical processes would desirable to separate Nb for the purpose of salt purification as well as volume reduction of radioactive waste, depending on the electrochemical behaviors for other elements that can be simultaneously dissolved with Nb.

© 2019 Published by Elsevier B.V.

1. Introduction

Niobium (Nb, Z = 41), one of the refractory metals, is commonly used as a minor alloying element for structural material in nuclear reactors. For example, it can be found in the zirconium alloy of the pressure tube of a pressurized heavy water reactor and fuel cladding, the nickel alloy of the part-strength control rod, or the steel of the reactor internal components, which should endure long periods

in harsh environments under high temperature, pressure, and neutron flux.

Nb-93, the most stable isotope of Nb, has a radiative capture (n, γ) cross-section of 1.02 b for thermal neutron and 28.4 mb for fast neutron at fission spectrum [1], and the generation of a small amount of Nb-94 is anticipated in the irradiated components. For instance, for the pressure tube (Zr-2.5Nb) exposed at the neutron flux of $1.0 \cdot 10^{14}$ n/cm²·sec for 30 effective full power years (EFPYs) in a pressurized heavy water reactor, the concentration of Nb-94 is estimated to be 0.69 wt% by ORIGEN-2 calculation, and it is negligibly decayed out during the cooling period, which is equivalent to the radioactivity of $8.38 \cdot 10^6$ Bg/g. It indicates that Nb-94, which

* Corresponding author.

E-mail address: jypark@unist.ac.kr (J. Park).

has a long half-life of 20,300 years [2], can contribute a large fraction of the total radioactivity for the waste containing Nb after service period of nuclear reactors as reported in Refs. [3,4]. Also, these characteristics could lead to the elevation of the radioactive waste hierarchy of the irradiated structural materials from the low-level waste to the intermediate level waste. While major concerns have been actively addressed for zirconium, iron, and nickel as the base metal [5], Nb has not been intensively dealt with in terms of the decontamination and long-term radioactivity management.

Electrolytic techniques in molten chloride and fluoride salts have been widely developed to separate and recycle valuable elements like U, Pu, and Zr from spent nuclear fuel and metallic radioactive wastes [5–8]. To adopt the electrolytic process as a decontamination technique for Nb-94 from radioactive waste, the electrochemical redox behavior of Nb should be clearly identified. Electrochemical behaviors of Nb have been shown to be relatively simple in fluorides or additive oxide salts [9–14]. However, the redox behavior in chloride salts has not yet been fully clarified and remains controversial due to the complexity from the multiple oxidation states and formation of nonstoichiometric insoluble Nb chloride compounds which are referred to as Nb subchlorides [15–28]. The endeavor to reveal their redox behavior in the chlorides has been pursued to take advantage of their low melting temperature and various options in choosing a salt container and electrode compared to fluoride salts at the laboratory scale [29].

Electrochemical behaviors of Nb ions have been studied in different molten chloride salts including NaCl–KCl [15–21], CsCl–NbCl [22–24], and LiCl–KCl [25–28]. Picard and Bocage identified that three ionic states, Nb(V), Nb(IV) and Nb(III), could exist in LiCl–KCl at 450 °C, and they calculated the apparent reduction potential for the reactions of Nb(V)/Nb(IV), Nb(IV)/Nb(III) and Nb(III)/Nb [25]. Lantelme et al. reported similar redox behaviors of Nb in LiCl–KCl at 450–630 °C with the three ionic states, and they additionally distinguished the existence of Nb subchlorides with non-stoichiometric numbers (NbCl_x with 2.33 < x < 3.13) which depended on the temperature [26]. They found that the oxidation potential of Nb subchlorides was more negative than that of Nb metal. However, Mohamedi et al. who explored redox behaviors of Nb ions in LiCl–KCl at 440 °C, argued that the oxidation potential of Nb subchlorides was found to be more positive than that of Nb metal [27], which is not consistent with other literature. In summary, the reduction behaviors of Nb ions, including the formation of Nb subchloride compounds and metallic Nb, were reported to be consistent, but the oxidation behavior of Nb metal and subchlorides were still questionable. In addition to the controversy over the reduction and oxidation behaviors of Nb ions, it is also arguable whether or not Nb(II) ions are involved in the formation of metallic Nb as well as Nb subchlorides.

In this study, the electrochemical behaviors of Nb in the molten LiCl–KCl–NbCl₅ at 450 °C were investigated by chronoamperometry (CA) and cyclic voltammetry (CV) with various scan rates and scan ranges. The X-ray diffraction (XRD) was also utilized to explore an ‘auto-reduction’ process between Nb(V) and Nb(IV). The possible reduction and oxidation reactions of Nb ions were determined by each peak information of the cyclic voltammograms. The reversibility and electrochemical properties, including the apparent reduction potential and diffusion coefficient, were also quantified for the identified redox reactions of Nb. The predicted redox behaviors and obtained values were compared to the previously reported results. Finally, the pyrochemical processes for different types of a radioactive waste containing Nb are suggested to examine the decontamination applicability for the waste while considering electrochemical behaviors of Nb and other metallic elements that can be dissolved from the waste during an electrolytic refinement.

2. Experimental setup

2.1. Electrochemical cell

An electrochemical cell containing pseudo-binary molten salt of LiCl–KCl with NbCl₅ was used for all experiments. These experiments were performed within a glovebox, which is designed to limit oxygen and moisture concentrations to less than 0.1 ppm in an Ar gas (99.99%) environment. An electrochemical cell for CV and CA, made of a Pyrex glass tube with a diameter of 11 mm and a height of 370 mm, was placed in an electric resistance furnace installed under the glovebox module as shown in Fig. 1. Also, another tube with the same dimensions as the electrochemical cell, containing pure LiCl–KCl salt and a K-type thermocouple, was placed right next to the electrochemical cell to measure the temperature. It was assumed that the temperature of salts within the two tubes are identical in the furnace after 12 h passed. The cell temperature was maintained at the desired temperature, 450 °C within ±1 °C, by a Proportional-Integral-Derivative (PID) controller connected to the furnace.

A metallic tungsten (W) wire (Alfa Aesar, 99.95%) with a diameter of 1.0 mm was used as a working and counter electrode. Tungsten wires were inserted into the cell with a Pyrex guide tube to hold stable positions and to avoid any undesirable contacts between the electrodes and the wall of the cell. For the reference electrode, Ag metal wire (Alfa Aesar, 99.99%) with a diameter of 1.0 mm was prepared and inserted into a Pyrex glass tube containing LiCl–KCl salt with 1.0 wt% AgCl (Alfa Aesar, 99.99%). The Pyrex glass tube had a thin tip (<0.5 mm thickness) in order to establish the ionic conduction between the solution and electrolyte. All electrode potentials in this study were referenced to this Ag/AgCl–LiCl–KCl (referred to simply as Ag/AgCl) unless specified otherwise. The surface of the metallic wire for the electrodes was mechanically polished, rinsed with anhydrous ethanol (Sigma-Aldrich, ≤0.005% water), and dehydrated for 2 h at 200 °C.

2.2. Chemicals and salt preparation

LiCl–KCl eutectic salt (Alfa Aesar, 99.99%) was heated for 24 h at 200 °C, lower than the melting point of 355 °C, to remove any residual moisture. Two salts of the dried LiCl–KCl and anhydrous NbCl₅ (Alfa Aesar, 99.99%) were mixed and melted simultaneously

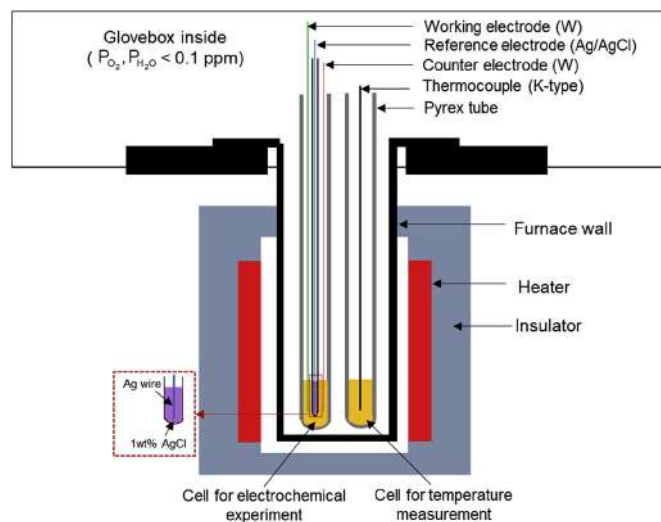


Fig. 1. Schematics showing a configuration of the electrochemical and temperature measuring cells in the glove box.

at 500 °C in order to prepare a salt mixture pellet containing a higher concentration of 10 wt% NbCl₅. The high-concentration pellet of LiCl–KCl–NbCl₅ was then diluted with pure LiCl–KCl beads which turned into a fused electrolyte. The preparation of the high-concentrated pellet was aimed at minimizing the volume of the reagent to be initially handled.

It was challenging to induce NbCl₅ into LiCl–KCl due to its high volatility and low boiling temperature (256 °C at 1 atm). The loss of some NbCl₅ during mixture preparation was inevitable, but it was minimized by rapidly inserting the Pyrex tube containing the salt mixture into the furnace at the high temperature of 500 °C and positioning NbCl₅ powder below the LiCl–KCl beads to capture as much NbCl₅ vapor as possible. The composition of the salt mixture was examined using inductively coupled plasma-optical emission spectrometry (ICP-OES), in which NbCl₅ content of 9.48 wt% was quantified. The color of the salt mixture was yellow-green, which is dependent on the amount of soluble Nb ions during quenching in the air to room temperature.

All electrochemical experiments were performed with the electrolyte of LiCl–KCl–1.0 wt% NbCl₅. The NbCl₅ content in the diluted electrolyte was measured for three different samples obtained from the fused salt in the cell by using ICP-OES again. Three salt samples were taken from three different cells in which the OCP reached a stable value. It should be noted that those cells were discarded and not utilized to conduct further electrochemical experiments. The results were 1.078, 1.019, and 0.936 in wt%, indicating that the salt mixture of LiCl–KCl–1.0 wt% NbCl₅ was reliably prepared within the acceptable measurement error and the NbCl₅ content measured by the ICP-OES represented the initial compositional state just before experiments applying voltage or current (e.g., cyclic voltammetry or chronoamperometry).

2.3. Experimental procedure

A VersaSTAT3 potentiostat, including the VersaStudio software package, was utilized to apply potential and current through three electrodes. A set of CVs were performed with CA at 450 °C and its objectives are summarized in Table 1: CV-1 to confirm the electrochemical potential window defined by the Li⁺ reduction and Cl[−] oxidation, CV-2 to identify all possible redox reactions in the LiCl–KCl–NbCl₅ system, CA-1 followed by CV-3, and CA-2 followed by CV-4 to identify the Nb(V)/Nb(IV) and Nb(IV)/Nb(III) redox reaction, respectively, and CV-5 to analyze the behaviors of the identified redox reactions by changing the scan rate.

The scan ranges set in CVs were selected based on the literature available in the molten LiCl–KCl containing Nb ions. As shown in Table 1, the CV scan range varied depending on the oxidation state of Nb ions introduced in the electrolyte. In our experiments, all cells used in CVs contained Nb(V) at the initial state, which means that

CVs with multiple cycles should be performed with the starting and ending potential which must be sufficiently positive to initialize the oxidation state of Nb ions as Nb(V) in the electrolyte. In this regard, the scanning for CVs was started and ended at 1.1 V (vs. Ag/AgCl), which is slightly less positive than the potential for the oxidation of Cl[−] (1.225 V vs. Ag/AgCl) [30].

Every CV was conducted by controlling the scan range and scan rate through the software interface. All experiments were carried out 1–2 days after inserting the electrodes into the cell to achieve the thermal equilibrium between the electrolyte and electrodes. It was assumed that they were in the thermal equilibrium when the measured open circuit potential (OCP) varied by less than 1.0 mV/h. Prior to changing the scan rate during CVs, the surface of the working electrode was anodically cleaned by applying a potential of 1.1 V (vs. Ag/AgCl) for 5 min to oxidize the metals and insoluble residues by turning them into dissolved ions. By the anodic polarization followed by the OCP measurement, it was safely assumed that only Nb(V) ions existed in the electrolyte in the initial state. After the anodic cleaning, the OCP of the cell was remeasured to ensure the equilibrium between the electrodes and electrolyte. Every CV was performed with at least 8 multiple cycles, and a repeatable voltammogram, which completely converged, was employed in the further analysis. Once CVs at different scan rates and a fixed scan range were completed, all electrodes and the cell were not further used, and they were replaced with new ones to avoid any interference caused by the previous experiment. For instance, all electrodes and the electrolyte used in the CV with a scan range from −0.2–1.1V (vs. Ag/AgCl) were replaced with to new ones before the next CV with a scan range from −0.3–1.1V (vs. Ag/AgCl).

Both CA-1 and CA-2 were performed for 12 h at the selected potentials which are specifically related to the reduction of Nb ions based on the literature and results from CV-2.

The surface area of the electrodes was determined after each experiment by measuring the immersion depth of the electrode since the height of the immersed part of the electrode was distinguished by residual salt deposits and the darker color. Although the same diameter of tungsten wire was used for the counter electrode as was used in the working electrode, the former was immersed deeper to avoid a counter-balancing electrochemical reaction limiting the process occurring at the working electrode. The surface area of the counter electrode was on average 1.46 times larger than that of the working electrode.

3. Results

3.1. Electrochemical window of the LiCl–KCl (CV-1)

CV-1 was performed to check the electrochemical window by

Table 1

A summary of the test matrix for different chronoamperometry (CA) and cyclic voltammetry (CV) with 1.0 wt% NbCl₅ in LiCl–KCl at 450 °C.

Test ID	Applied potential or scan range (V vs. Ag/AgCl)	Scan rate (mV·sec ^{−1})	Purpose
CV-1	−2.0–0.8 −2.2–1.0 −2.4–1.2 −2.6–1.4	300	Confirm electrochemical window of the pure LiCl–KCl
CV-2	9 ranges from −0.2–1.1 to −1.0–1.1	300	Identify all possible redox reactions
CA-1	0.6	–	Reduce Nb(V) to Nb(IV)
CA-2	−0.05	–	Reduce Nb(V) and Nb(IV) to Nb(III)
CV-3	0.6–1.1	30, 50, 80, 100, 300, 500, 700, 1000, 1500	Determine the redox reaction for Nb(V)/Nb(IV) and diffusion coefficient of Nb(V)
CV-4	−0.1–0.7		Determine the redox reaction for Nb(IV)/Nb(III) and diffusion coefficient of Nb(IV)
CV-5	9 ranges from −0.2–1.1 to −1.0–1.1		Examine the behaviors of redox reactions identified by CV-2

using a pure salt of LiCl–KCl at 450 °C. The stable electrochemical domain was restricted by the Li reduction on the cathodic wave and the evolution of Cl₂ gas on the anodic wave. The stable electrochemical domain was defined from –2.50–1.22 V with acceptable limits of the current densities less than ±5 mA·cm^{–2}. The performance of the reference electrode was validated because the measured electrode potential for Cl₂ gas evolution at 1.223 V was consistent with the reported potential of 1.225 V in the literature [30].

3.2. Chronoamperometry for the stability of Nb ions

Fig. 3 shows the measured current changes for CA-1 designed to reduce Nb(V) into Nb(IV) at 0.6 V for 12 h following the 10-min anodic stripping electrode cleanout at 1.1 V. It can be noticed that the anodic current decreased initially during the cleanout but continued to increase slightly over time. In addition, during the following step of CA-1 in order to reduce Nb(V) to Nb(IV), the cathodic current density reached 0.66 mA·cm^{–2} within 30 s and remained stable until the termination. Based on this observation, it was questionable which of the oxidation states of Nb ions was dominantly present prior to each electrochemical experiment.

Fig. 4 shows the color of the salt electrolyte that contained Nb ions with different oxidation states. It was assumed that all Nb ions existed as Nb(V) when the cell was initially prepared, as shown in Fig. 4(b). When CA-2 was performed for 12 h at –0.05 V to reduce both Nb(V) and Nb(IV) to Nb(III), it was found that the color of the Nb solution changed from dark orange to light gray as the concentration of Nb ions with a lower oxidation state increased. The color change of the Nb solutions was consistent with the literature: orange for a higher oxidation state close to 4 and gray for an oxidation state lower than 3.8, as reported by Picard and Bocage [25], Lantelme et al. [26], and Mohamedi et al. [27]. Since all cells used in the CVs had an orange-colored molten salt, Nb(V) was believed to be the most stable species during all the CVs in this study.

3.3. Identification of all possible redox reaction

3.3.1. Cyclic voltammograms with various scan ranges (CV-2)

We performed CV-2 to identify possible redox reactions in LiCl–KCl–NbCl₅ molten salt as represented in Fig. 5. In CV-2, nine

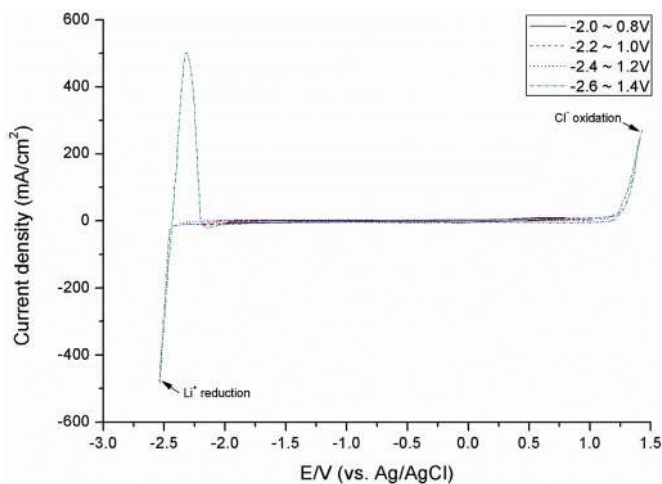


Fig. 2. Cyclic voltammograms with a pure LiCl–KCl at 450 °C (scan rate = 300 mV·s^{–1}, working and counter electrode = tungsten wire, reference electrode = Ag/AgCl, surface area = 0.48 cm²).

different scan ranges were selected with fixing the starting potential as 1.1 V and changing switching potential from –0.2 to –1.0 V. Four reduction peaks (R1 ~ R4) and five oxidation peaks (O1 ~ O5) were found, which were distinguished by the rate of changes in the current density. Possible redox reactions for each peak are also presented in this paper. The R1 and O5 peaks were challenging to find due to the lower magnitude of their current density compared to the others as the scan range increased. The current density recorded around the potential of 1.1 V at which the scanning started and ended in each voltammogram appeared to be affected by the oxidation of Cl[–] to Cl₂ gas, occurring at a potential of 1.22 V as mentioned in the previous section.

When the switching potential in the scan ranges was more positive than –0.3 V (e.g., scan range of –0.2–1.0 V), only two redox peak pairs (R1/O5 and R2/O4) were found on each cathodic and anodic wave. These four peaks have a broad shape which indicates that these redox couples involve electrochemical reactions controlled by the diffusion of a soluble species.

Peak behaviors became complicated due to the multiple oxidation states of Nb ions when the switching potential in the scan range expanded from –0.5 to –1.0 V. In particular, the shapes of the oxidation peaks during the anodic sweep changed noticeably as three oxidation peaks (O1, O2, and O3) started to emerge with two additional reduction peaks (R3 and R4). The oxidation peak of O1 and O2 can be attributed to the oxidation reaction of insoluble reactants, occurring at the surface of electrodes due to the sharp rise of the oxidation current density. Two reduction peaks (R3 and R4) were differentiated by the rate of the potential shift as a function of the logarithm of the scan rate, although they appeared to overlap as presented in Section 4.2.

As the switching potential was expanded from –0.5 to –0.6 V, an abrupt shift in the peak potential for R3 was found from –0.478 to –0.530 V, which may indicate that a different reduction reaction related to the peak of R4 occurred. It would also imply that those two reactions competed with each other. However, when the switching potential was more negative than –0.7 V, only the R4 peak was observed. The characteristics of each redox peak were examined by additional sets of cyclic voltammetry (CV-3 ~ CV-5) employing different scan ranges and scan rates.

3.3.2. Examination of Nb(V)/Nb(IV) and Nb(IV)/Nb(III) redox reaction (CV-3 and CV-4)

Fig. 6 shows the voltammogram of CV-3 and CV-4 with narrow scan ranges to focus on the redox couples of (R1/O5) and (R2/O4) related to Nb(V)/Nb(IV) and Nb(IV)/Nb(III), respectively. The peak current density at each peak potential of R1 and R2 showed linearity, depending on the square root of the scan rate. As shown in Fig. 7, the interpolation line passes through the origin, which indicates that the two redox reactions are part of a reversible diffusion-controlled process between the two soluble ions. It is noticeable that the slope of the peak current density for R2 as a function of the square root of the scan rate is steeper than that for R1.

The comparison of the current density at the cathodic and anodic peak of a coupled redox reaction can be used to diagnose the reversibility of the reaction. However, the peak current density for O5 was difficult to quantify since the peak potential for O5 was very close to the potential of the evolution of Cl₂ gas, while that for R1 was obtained by subtracting the background current density (2.85 mA·cm^{–2}) obtained from the CV with setting the baseline to zero. For the R2/O4 redox couple, the peak current density for R2 (*I*_{p,c}) and O4 (*I*_{p,a}) at a scan rate of 1500 mV·s^{–1} which are denoted in Fig. 6(b), was measured with the baseline. As a result, the ratio of *I*_{p,c} to *I*_{p,a} was 0.784, deviating from the unity, which implies the diffusion coefficient of the reduced species might be higher than

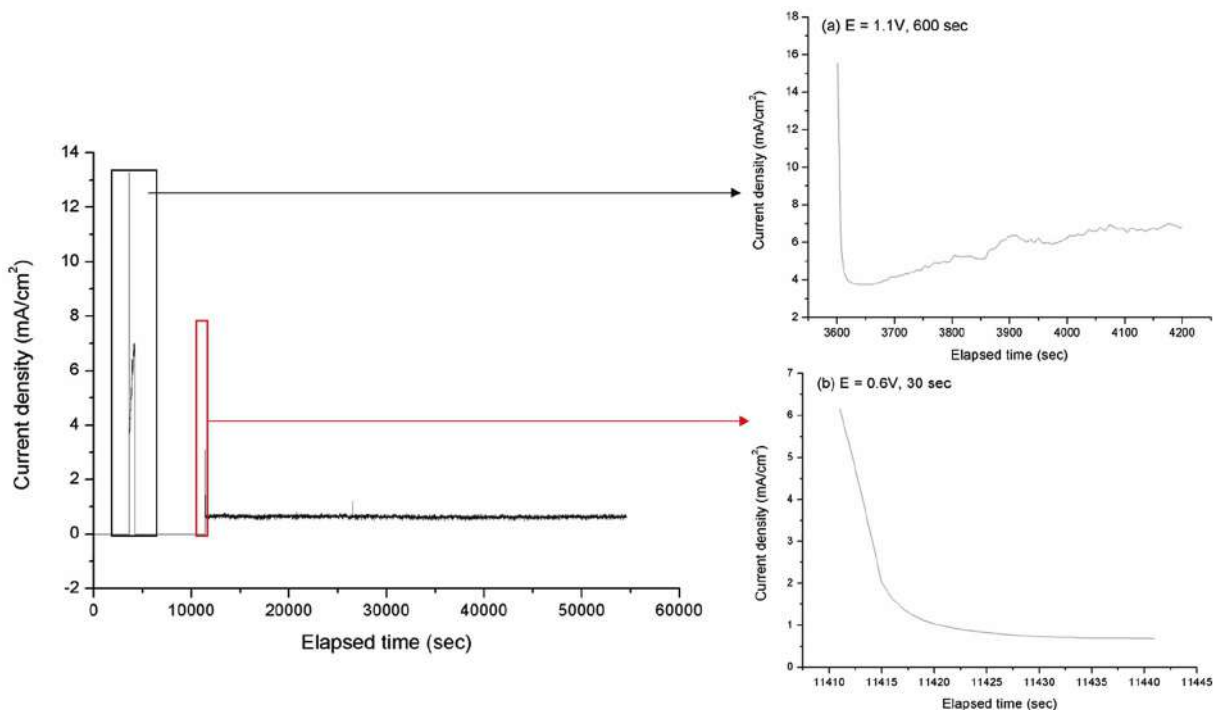


Fig. 3. Measurement of current during at a potential of (a) 1.1 V for the anodic cleaning of the electrode and (b) 0.6 V for the reduction of Nb(V) to Nb(IV) during CA-1.

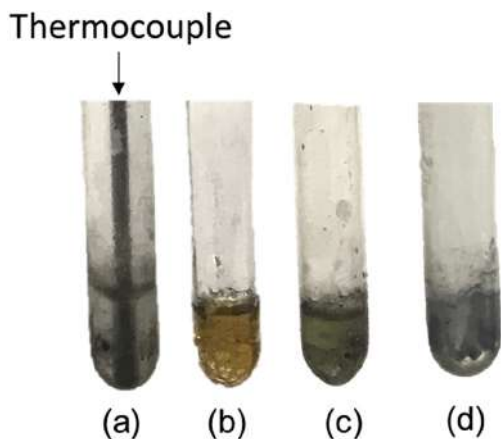


Fig. 4. Colors of Nb-containing solutions with the different oxidation states of Nb ion at 450 °C; (a) a pure LiCl–KCl, LiCl–KCl with 1.0 wt% NbCl₅ (b) before CA-1, (c) after CA-1, and (d) after CA-2. (For interpretation of the references to color in this figure legend, the reader is referred to the Web version of this article.)

the oxidized one.

Since the peak-to-peak separation for both coupled reactions did not vary significantly as a function of the scan rate, indicating that both reactions are reversible.

3.3.3. Examination on peak behaviors (CV-5)

It was found that all current densities at peak potentials for the reductions proportionally increased as the scan rate increased. As shown in Fig. 8(a) and (b), a reduction peak started to grow at a potential near to -0.4 V. This peak R3 became clearly observable when the scan rate was lower than $300 \text{ mV} \cdot \text{s}^{-1}$ and the switching potential expanded from -0.4 to -0.5 V. However, it became blurred when the scan rate became higher than $500 \text{ mV} \cdot \text{s}^{-1}$. When the potential scanning was performed toward a more negative

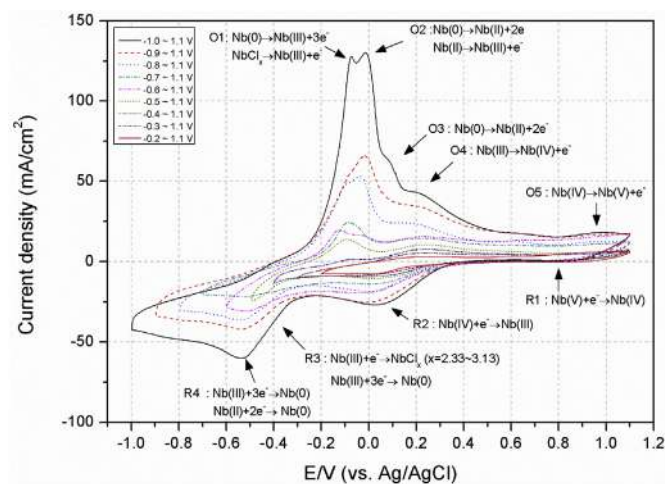


Fig. 5. Voltammograms showing all possible redox reactions with identifiable current peaks (Scan rate = $300 \text{ mV} \cdot \text{s}^{-1}$).

direction, the peak R3 became indistinguishable, while the peak R4 was viable. It also appeared that the peak R3 stopped growing as the scan rate increased.

Noticeable changes in the shape of the oxidation peaks were found as the scan range became broader. The peak O1 started to emerge (Fig. 8(a)) and continuously grew (Fig. 8(b)) with the switching potential of -0.4 and -0.5 V. In the scan range from -0.6 – 1.1 V as shown in Fig. 8(c), the peak O1 appeared distinctly, until the scan rate dropped to less than $300 \text{ mV} \cdot \text{s}^{-1}$. As the scan rate increased, another anodic peak O2 was observed at the right side of peak O1 and arose together with peak O2. This competition between the two peaks is clearly shown in Fig. 9. At the low scan rate, the height of O1 is higher than that for O2, but the tendency was transposed, in that peak O2 became apparently

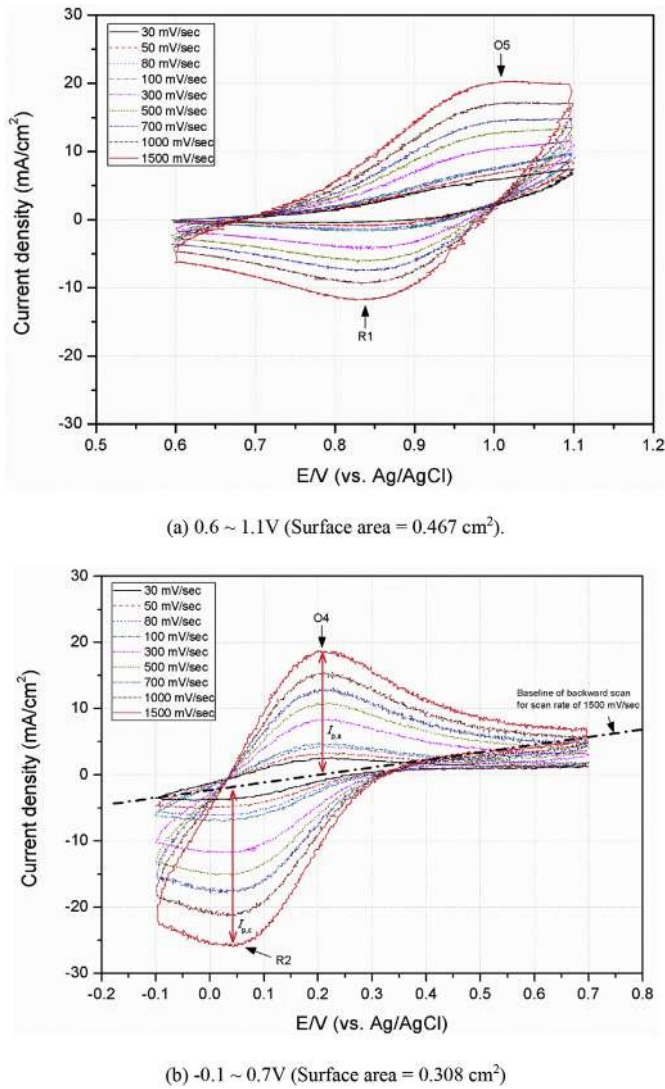


Fig. 6. Voltammograms with different scan ranges and scan rates showing two redox reactions of (a) Nb(V)/Nb(IV) and (b) Nb(IV)/Nb(III).

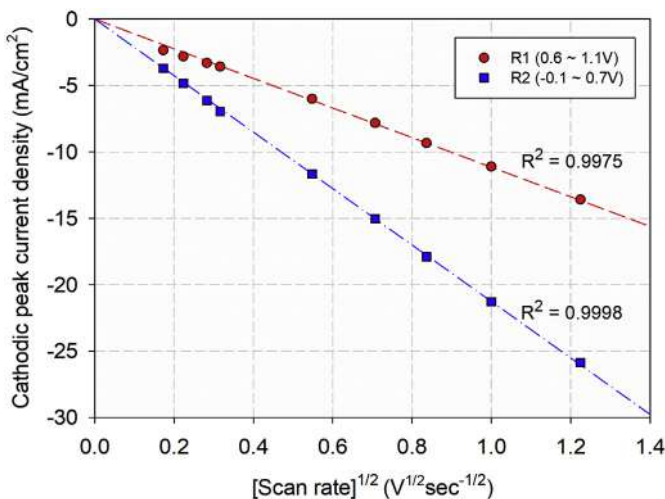


Fig. 7. Cathodic peak current density as a function of the square root of scan rate for R1 and R2.

dominant with scan rates higher than $500 \text{ mV} \cdot \text{s}^{-1}$. When the negative limit reached -0.7 V , these two peaks could not be distinguished due to the steep height of peak O2 which rapidly grew and turned into a new peak (Fig. 8(d)). Peak potentials shifted depending on the scan rate changes; there was a negative shift in R3 and R4, and a positive shift in O1, O2, and O3.

The growth of peak O4 and O5 appeared to be affected by the formation of peak O2; the current densities of peak O4 and O5 showed a tendency to increase slightly until peak O2 was observed, as shown in Fig. 8(a) and (b). As the scan range became broader, however, their peak heights grew aggressively as the scan rate became higher.

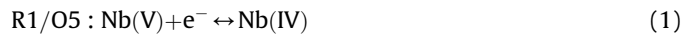
When the negative limit of the scan was less than -0.9 V , peak O1, and O2 appeared to merge, and a new peak, O3, became viable at a right shoulder of peak O2, as shown in Fig. 9. The peak O3 was observed at scan rates lower than $300 \text{ mV} \cdot \text{s}^{-1}$, but it became obscure at high scan rates due to the anodic trace next to peak O2 by diffusion of the oxidized species from the electrode to the bulk electrolyte.

4. Discussion

4.1. Peak current density analysis for Nb(V)/Nb(IV) and Nb(IV)/Nb(III)

In cases where the current density of a specific reaction can be measured with the known molar concentration of an analyte, it is possible to estimate the diffusion coefficient of the species involved in the reaction. In this study, the background current density was measured to be less than $2.8 \text{ mA} \cdot \text{cm}^{-2}$ in the eutectic LiCl–KCl base electrolyte in Fig. 2. This background data was used to obtain the peak cathodic current density for R1 and R2, described in Fig. 6.

Only two couples of redox reactions (R1/O5 and R2/O4) were observed when the scanning was performed with the range of -0.3 – 1.1 V , as mentioned in Section 3.3.2. The potentials of these cathodic and anodic peaks were well-matched to those of the redox reactions for Nb(V)/Nb(IV) and Nb(IV)/Nb(III) reported by Salmi et al. [18] and Lantelme et al. [26] based on the shape of the voltammograms and the diffusion-controlled characteristics. Thus, the possible reactions for R1/O5 and R2/O4 are given by Eqs. (1) and (2) as follows:



Diffusion coefficients for Nb(V) and Nb(IV) were calculated to confirm the validity of the conducted experiment with a comparison to the literature data. For the reversible soluble-soluble reaction, the Randles-Sevcik equation was used to calculate the diffusion coefficient of dissolved species when the peak current is known as follows [31]:

$$i_p = 0.446nFAC^0 \left(\frac{nFvD_0}{RT} \right)^{1/2} \quad (3)$$

where i_p is the current at the peak potential in A, n is the number of transferred electron during the reaction, A is the surface area of the electrode in cm^2 , C^0 is the bulk concentration of the species involved in the reaction in $\text{mol} \cdot \text{cm}^{-3}$, F is the Faraday constant, D_0 is the diffusion coefficient of the species in $\text{cm}^2 \cdot \text{sec}^{-1}$, R is the gas constant, and T is the temperature in K.

The calculated results for the diffusion coefficient of Nb(V) and Nb(IV) using Eq. (3) are summarized in Table 2. A direct comparison of diffusivity among Nb ions is not possible due to the lack of

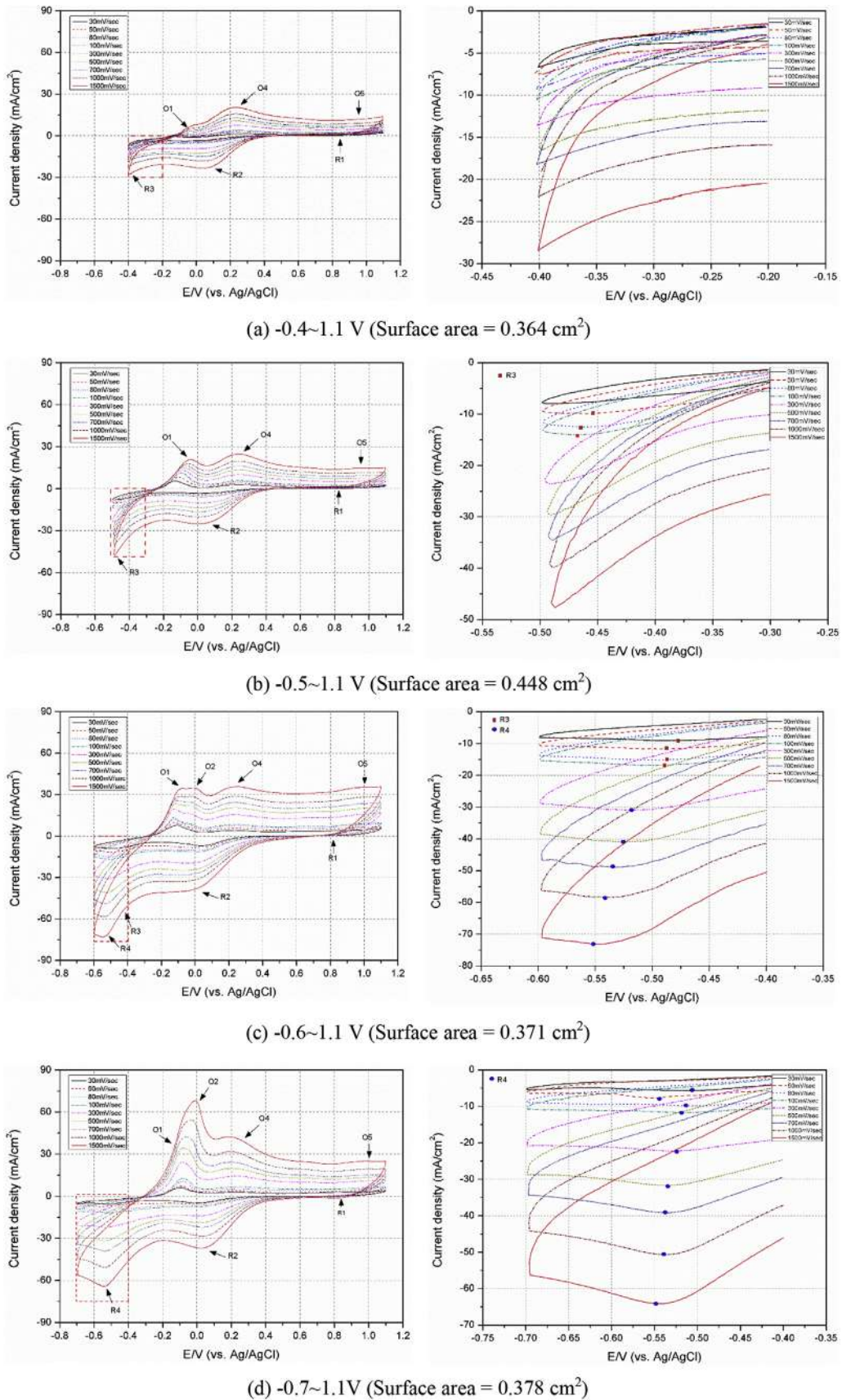


Fig. 8. A set of voltammograms with different scan ranges at different scan rates (left-side) and voltammograms with the narrow scan range marked as red-dotted box (right-side). (For interpretation of the references to color in this figure legend, the reader is referred to the Web version of this article.)

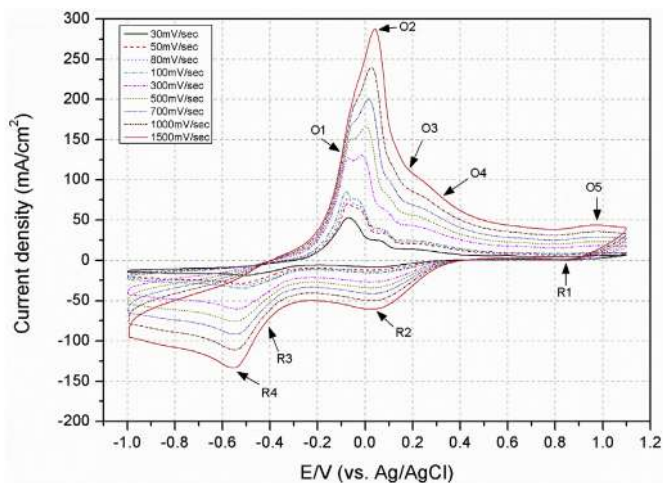


Fig. 9. Voltammograms showing the behavior of observed peaks in the scan range from -1.0 – 1.1 V at different scan rates (Surface area = 0.475 cm^2).

available data, but the results show that the diffusion coefficient of Nb(V) was much lower than that for Nb(IV). Thus, it entails a higher current density of the anodic peak O1 than that of the cathodic peak R5, shown in Fig. 6(a).

Lantelme et al. calculated the diffusion coefficient of Nb(IV) by using chronopotentiometry (CP) to measure the transition time for the recorded potential of a vitreous carbon electrode in Nb(III) solution [26]. They found that Nb(IV) and Nb(III) had approximately the same diffusion coefficient. Then, the diffusion coefficient of Nb(III) reported by Mohamedi et al. [27] can also be compared to the result of this study. The obtained diffusion coefficients of Nb(IV) and Nb(V) from the present study are in the same order and well matched to the value reported by Mohamedi et al. but Nb(IV) is shown to have lower diffusivity than the value derived by Lantelme et al.

During the CP conducted by Lantelme et al. it was found that the number of electrons (n) transferred for the anodic reaction Nb(III) and Nb(IV) deviated from the unity, varying from 0.7 to 0.9, due to the formation of an NbC compound on the electrode surface. Thus, it is believed that the lower value of n induces the overestimation of the diffusion coefficient of Nb(IV) reported by Lantelme et al. [26].

Based on the observation where the ratio of the peak current densities ($I_{p,a}/I_{p,c}$), denoted in Fig. 6(b), was lower than the unity, the diffusion coefficient of Nb(III) appeared to be lower than that of Nb(IV). Thus, the discrepancy between the diffusion coefficient of Nb(IV) obtained from this study and that of Nb(III) reported by Mohamedi et al. [27] might be acceptable. Despite the discrepancy

in the diffusion coefficient of Nb(IV) which can be largely dependent on the different experimental conditions and reagents used, the obtained results indicate that the CV experiments were reliably performed in the present study since they have the same magnitude as the available literature data.

4.2. Peak potential analysis

The peak potentials (E_p) recorded during the CVs are the unique potentials that can be used to analyze the electrochemical behaviors of analytes. They are useful when the concentrations of dissolved species are unknown, and the peak current density is difficult to measure due to the complex behavior of the redox peaks.

Fig. 10 shows the peak potentials measured by CV-2, -3, -4, and -5 as a function of the logarithm of the scan rate. The peak potentials of R1 and R2 did not vary as a function of the logarithm of the scan rate. The average separation of potentials for the redox couple (R1/O5) is 140.1 mV , which is well matched to the theoretically derived value of the peak-to-peak separation by 2.218 RT/F . However, the average peak-to-peak separation for the redox couple (R2/O4) is 242.5 mV , deviating from the theoretical value, which is similar to the CV results reported by Lantelme et al. [26]. This implies that the Nb(IV)/Nb(III) redox reaction is quasi-reversible, which possibly shows the reversible behaviors at the scan rates used in this study.

The shifts of other peak potentials as a function of the logarithm of the scan rate are clearly shown in Fig. 10(b) and (d). These shifts indicate that electrochemical reactions related to those peaks are irreversible. The shift of the peak potential is given as a function of the logarithm of the scan rate for the irreversible process as follows [31]:

$$\left| \frac{dE_p}{d \ln \nu} \right| = \frac{RT}{2\alpha nF} \quad (4)$$

where ν is the scan rate in $\text{V} \cdot \text{sec}^{-1}$, α is the charge transfer coefficient assumed to be 0.5, n is the number of electrons transferred in a reaction, R is the gas constant, T is the temperature in K, and F is the Faraday constant. Using Eq. (4), it is possible to obtain the number of electrons (n) transferred during the reaction of each peak when the slope of $\left| \frac{dE_p}{d \ln \nu} \right|$ is known. The calculated results are summarized in Table 3.

The calculated n for each peak varied depending on the scan range. This implies that a reaction occurred with multiple steps or at least two reactions competed with each other. The calculation results for the number of the transferred electron are determined

Table 2
Comparison of the diffusion coefficient of Nb ions in molten LiCl–KCl.

Scan rate ($\text{mV} \cdot \text{sec}^{-1}$)	Cathodic peak current density ($\text{mA} \cdot \text{cm}^{-2}$)		Diffusion coefficient ($10^{-6} \text{ cm}^2 \text{ s}^{-1}$)			
	R1 from Fig. 6 (a)	R2 from Fig. 6 (b)	This study	Lantelme et al. [26]	Mohamedi et al. [27]	
			Nb(V)	Nb(IV)	Nb(IV) ^a	Nb(III)
30	2.35	3.70	1.10	2.73	5.42	2.60
50	2.82	4.83	0.95	2.79		
80	3.30	6.13	0.82	2.81		
100	3.58	6.96	0.77	2.90		
300	6.01	11.66	0.72	2.71		
500	7.83	15.04	0.73	2.71		
700	9.34	17.91	0.75	2.74		
1000	11.10	21.29	0.74	2.71		
1500	13.59	25.86	0.74	2.70		

^a Reported that $D_{\text{Nb(IV)}} = D_{\text{Nb(III)}}$.

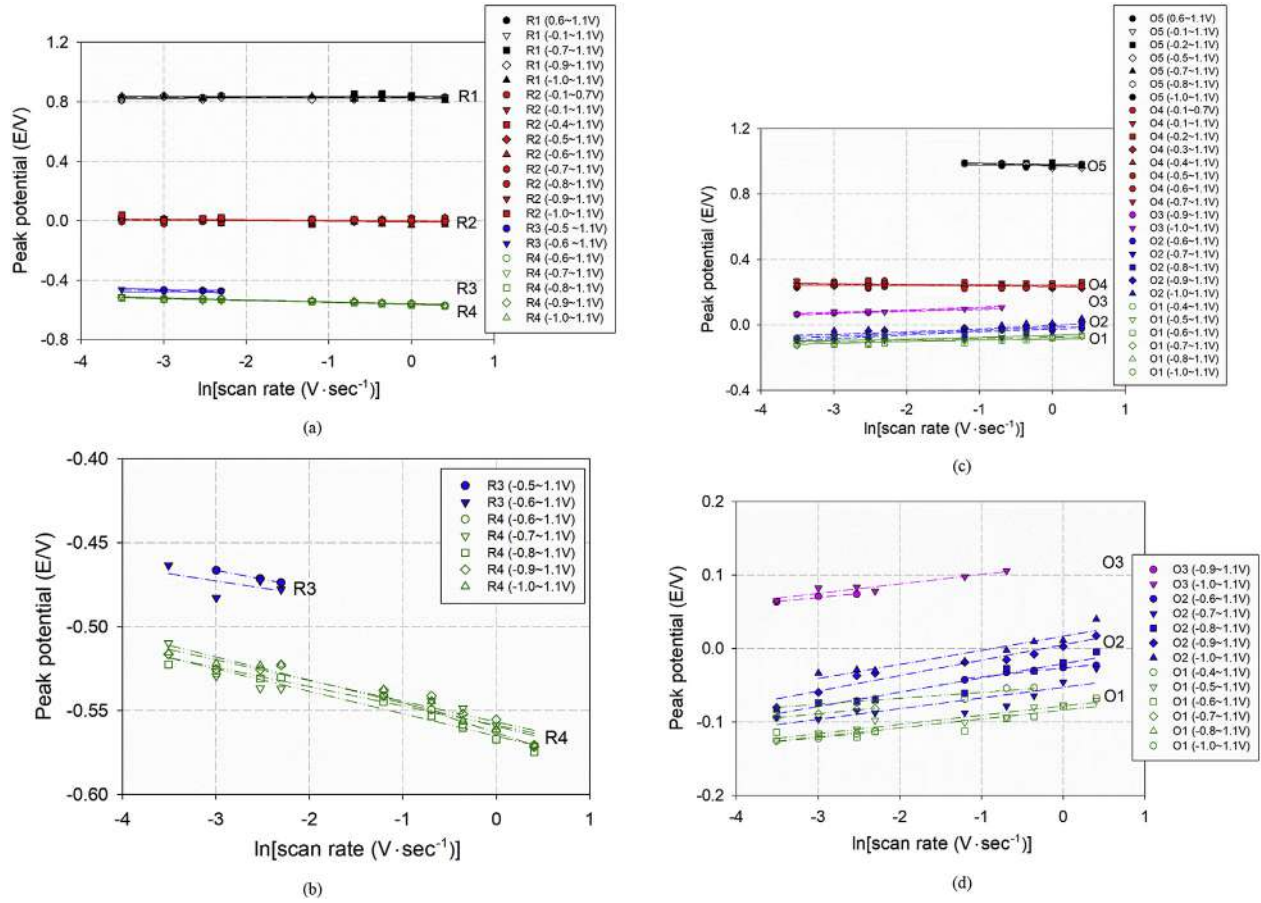


Fig. 10. Dependency of peak potentials for (a) all reduction peaks, (b) R3 and R4, (c) all oxidation peaks, and (d) O1, O2, and O3 on the logarithm of the scan rate with different scan ranges.

Table 3

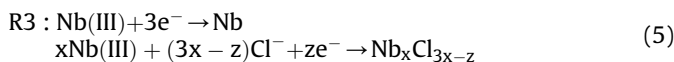
Summary of the calculated number of transferred electrons in each reaction.

Scan range	The number of transferred electrons (n) involved in reactions ^a				
	Peaks				
	R3	R4	O1	O2	O3
-0.4–1.1V			2.51		
-0.5–1.1V	2.38		2.15		
-0.6–1.1V	3.17		2.24	2.28	
-0.7–1.1V		2.35	2.56	1.86	
-0.8–1.1V		2.04		1.39	
-0.9–1.1V		2.19		1.26	2.04
-1.0–1.1V		1.97		1.32	2.10
Average n	2.77	2.15	2.56	1.62	2.07

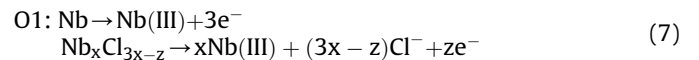
^a Assumed that $\alpha = 0.5$.

by the reaction which occurred more dominantly or the rate-controlling reaction in multiple steps [31]. Possible reactions can be given by Eqs. (5)–(9) based on the number of transferred electrons and a comparison with the literature as follows:

- For the cathodic peaks:



- For the anodic peaks:



where $1 \leq z \leq 2$ is satisfied. All possible redox reactions for each peak are summarized in Table 4 by a comparison of all the available cyclic voltammograms including this study and other literature [18,25–27].

The number of electrons involved in the reduction reaction for the peak R3 varied complicatedly. The peak potential for R3 overlapped with that for R4 when the switching potential ranged from -0.5 to -0.7 V, which indicates the transition of reduction behaviors for the deposit formation from Nb subchlorides to the metallic Nb at the electrode surface. The deposition of Nb subchlorides, which hindered the deposition of the metallic Nb, has been reported in the literature [20,26–28].

The direct reduction of Nb ions, including Nb(III) and Nb(II), is

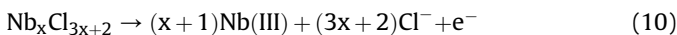
Table 4
Possible reactions for each anodic and cathodic peak in LiCl–KCl molten salt.

	Present study	Picard and Bocage [25]	Lantelme et al. [26]	Lantelme et al. [18]	Mohamedi et al. [27]
Cell	WE = Tungsten RE = Ag/AgCl (1.0 wt%) LiCl–KCl–NbCl ₅ C _{Nb⁵⁺} = 7.45 × 10 ⁻⁵ mol·cm ⁻³ T (°C) 450	WE = Tungsten RE = Ag/AgCl (0.75 mol·kg ⁻¹) C _{Nb³⁺} = 3.2 × 10 ⁻² mol·kg ⁻¹ by anodic dissolution 450	WE = Vitreous carbon and molybdenum RE = Cl ₂ /Cl ⁻ C _{Nb^{m+}} = 5.0 × 10 ⁻² , = 7.2 × 10 ⁻² mol·L ⁻¹ by anodic dissolution 450	WE = Niobium RE = Cl ₂ /Cl ⁻ C _{Nb³⁺} = 2.0 × 10 ⁻⁶ mol·cm ⁻³ 550	WE = Tungsten RE = Ag/AgCl (5 mol %) LiCl–KCl–Nb ₃ Cl ₈ C _{Nb^{m+}} = 1.5 × 10 ⁻⁵ mol·cm ⁻³ 440
Anodic peak					
O1	Nb → Nb(III) + 3e ⁻ Nb _x Cl _y → Nb(III)	Nb → Nb(III) + 3e ⁻	Nb _x Cl _y → Nb(III)	Nb _x Cl _y → Nb(III)	Nb → Nb(II) + 2e ⁻
O2	Nb → Nb(II) + 2e ⁻ Nb(II) → Nb(III) + e ⁻		Nb → Nb(III) + 3e ⁻		Nb _x Cl _y → Nb(III)
O3	Nb → Nb(II) + 2e ⁻				
O4	Nb(III) → Nb(IV) + e ⁻		Nb(III) → Nb(IV) + e ⁻	Nb(III) → Nb(IV) + e ⁻	Nb(III) → Nb(IV) + e ⁻
O5	Nb(IV) → Nb(V) + e ⁻	Nb(IV) → Nb(V) + e ⁻	Nb(III) → Nb(IV) + e ⁻	Nb(IV) → Nb(V) + e ⁻	
Cathodic peak					
R1	Nb(V) + e ⁻ → Nb(IV)	Nb(V) + e ⁻ → Nb(IV)	Nb(V) + e ⁻ → Nb(IV)		
R2	Nb(IV) + e ⁻ → Nb(III)		Nb(IV) + e ⁻ → Nb(III)		Nb(III) + e ⁻ → Nb(II)
R3	Nb(III) → Nb _x Cl _y Nb(III) + 3e ⁻ → Nb	Nb(III) + 3e ⁻ → Nb	Nb(III) → Nb _x Cl _y	Nb(II) + 2e ⁻ → Nb	Nb(III) → Nb _x Cl _y
R4	Nb(II) + 2e ⁻ → Nb		Nb(III) + 3e ⁻ → Nb		Nb(II) + 2e ⁻ → Nb

believed to occur at the peak R4. It has been reported that the reduction of Nb species into the metal occurs via two electrochemical steps; a reversible one-electron-transfer step, and a two-electron-transfer step that is irreversible [27]. Although the one-electron reversible step was not viable in this study, the reduction of Nb(II) to the metallic Nb was found in this study. It appears that the direct reduction of Nb(II) was the rate-controlling step to determine the kinetics of the deposition of the metallic Nb.

For the oxidation peaks, it is believed that the peak O1 was caused by the oxidation of the Nb subchlorides based on a comparison with the literature. Still, it is not possible to identify the number of electrons involved in both the formation and dissolution of Nb subchlorides. Lantelme et al. reported that Nb subchloride compounds are produced via a one-electron transfer step, and the rest of the oxidation valence is completed by the chlorine ion [26]. Thus in our study, the metallic Nb was oxidized to Nb(III) or Nb(II) simultaneously at the peak O1, based on the calculated number of transferred electrons.

In our experiment, the peak O2 appeared to have either the one- or two-electron transfer step, which possibly involved the oxidation of the metallic Nb to Nb(II) or Nb(II) to Nb(III). The oxidation of the metallic Nb occurred at the surface of the electrode, which means it was not a diffusion-controlled process. Based on the calculated number of the transferred electron for the peak O2, one can argue that it was due to the oxidation of the Nb subchloride compound as follows:



Mohamedi et al. mentioned that the peak O2 was caused by the oxidation of insoluble Nb chloride compounds [27], which is inconsistent with the results by Lantelme et al. [26]. However, since the deposition of metallic Nb is known to be promoted as the more negative potential is applied, the rapid increase in the height of peak O2 is strongly related to the oxidation of the metallic Nb with the multiple electron transfer steps. Besides, the oxidation of Nb(II) to Nb(III) with the one-electron transfer step is highly likely to be the rate-controlling step at the peak O2.

Despite the lack of data for peak O3, an irreversible two-electron step was found for the peak O3. This was possibly due to the oxidation of the metallic Nb into Nb(II), since this peak was only found when the negative limit of the scan range was less than -0.9 V where the deposition of the metallic Nb was predominant.

In order to obtain the peak-to-peak separation of a possible redox reaction, the redox couple was hypothetically presumed based on the calculation results and a comparison to the literature data as follows: R3/O1 for Nb(III)/NbCl_x, R4/O2 for Nb(III)/Nb, and R4/O3 for Nb(II)/Nb.

Table 5 shows a summary of the apparent standard potential of redox reactions for Nb in the molten LiCl–KCl. All available formal potentials are converted into potentials with respect to the Cl₂/Cl⁻ reference electrode by the extrapolation of the data of Yang and Hudson [32] at low AgCl concentrations in LiCl–KCl eutectic as an infinitely dilute solution with a unit activity of the pure metal as follows:

$$E_{\text{Ag/AgCl}} / \text{V (vs. Cl}_2/\text{Cl}^-) = E_{\text{AgCl}}^0 + \frac{2.303RT}{F} \log X_{\text{AgCl}} \quad (11)$$

where X_{AgCl} is the mole fraction of AgCl in LiCl–KCl eutectic ($X_{\text{AgCl}} = 0.0039$ for 1 wt% AgCl), R is the gas constant, and T is the temperature in K. E_{AgCl}^0 relative to the Cl₂/Cl⁻ reference electrode is given by Fusselman et al. [30] as follows:

$$E_{\text{AgCl}}^0 = -1.0910 + 2.924 \times 10^{-4}T \quad (12)$$

where T is the temperature in K.

In the case of a reversible electrode reaction, the cathodic peak potential (E_{pc}) depends on the formal potential (E^0) as follows:

$$E_{\text{pc}} = E^0 - 1.109 \frac{RT}{nF} - \frac{RT}{nF} \ln \frac{D_{\text{ox}}^{1/2}}{D_{\text{red}}^{1/2}} \quad (13)$$

where D_{ox} and D_{red} are the diffusion coefficient of oxidized and

Table 5
Comparison of formal potentials (vs. Cl_2/Cl^-) for each redox reaction in Nb-containing LiCl–KCl.

Method	Temperature (°C)	Formal potential (E^0) for redox reactions (E/V vs Cl^-/Cl_2) at 450 °C						Ref.	
		Solute	Exp.	Nb(II)/Nb	Nb(III)/Nb	Nb(III)/NbCl _x	Nb(III)/Nb(II)		Nb(IV)/Nb(III)
Nb metal dissolved ($0.17 \cdot 10^{-6} \text{ Nb}^{3+} \text{ mol/cm}^3$)	CV	445	-1.54	-1.42		-1.16		[18]	
Nb metal dissolved	OCP ^a , LSV ^b	450		-1.44			-1.12	-0.32	[25]
Nb metal dissolved ($5 \cdot 10^{-2} \text{ mol/liter}$)	CV	450		-1.48		-1.32	-1.09	-0.32	[26]
NbCl ₅ ($7.45 \cdot 10^{-5} \text{ Nb}^{5+} \text{ mol/cm}^3$)	CV	450	-1.61	-1.55	-1.50		-1.11	-0.32	Present study

^a Open-circuit potential.

^b Linear sweep voltammetry.

reduced species in $\text{cm}^2 \cdot \text{sec}^{-1}$, respectively, and T is the temperature in K.

The formal potentials for redox couples of Nb(V)/Nb(IV) and Nb(III)/Nb(IV) were determined with known reduction and oxidation peak potentials (R1, R2, and O4, O5). Assuming that the diffusion coefficient of Nb(IV) and Nb(III) are equal, then Eq. (13) turns into a simple relation given as follows:

$$E^0 = \frac{E_{\text{pa}} + E_{\text{pc}}}{2} = E_{1/2} \quad (14)$$

where E_{pa} is the anodic peak potential in V, and $E_{1/2}$ is the half-wave potential in V.

In the case of an irreversible reaction, only the reduction peak can be employed, which depends on the formal potential as follows:

$$E_{\text{pc}} = E^0 + \frac{RT}{\alpha n F} \left(0.780 + 0.5 \ln \frac{\alpha n D_{\text{ox}} F \nu}{RT} - \ln k_s \right) \quad (15)$$

where k_s is the standard rate constant of the electrode reaction in $\text{cm} \cdot \text{sec}^{-1}$, and ν is the scan rate in $\text{V} \cdot \text{sec}^{-1}$. For the case where the peak-to-peak separation (ΔE_p) is larger than 200 mV, a relationship reported by Klingler and Kochi [33] can be used to estimate k_s as follows:

$$k_s = 2.18 \left(\frac{\alpha n D_{\text{ox}} F \nu}{RT} \right)^{1/2} \exp \left[- \left(\frac{\alpha^2 n F}{RT} \cdot \Delta E_p \right) \right] \quad (16)$$

The calculation of the diffusion coefficient of Nb(II) and Nb(III) was not possible due to the fact the concentration of those Nb ions cannot be quantified during the experiment. Thus, it was assumed that the diffusion coefficient of Nb(II), Nb(III) and Nb(IV) were identical.

The calculated formal potentials for the redox couples of Nb(IV)/Nb(III) and Nb(V)/Nb(IV) are in good agreement with the literature data, but there are discrepancies within ± 0.1 V among those for Nb(II)/Nb and Nb(III)/Nb. It was difficult to compare the formal potentials, particularly for the reaction in which the concentration of the dissolved species was unknown, including R3 and R4 in the cathodic wave, and O1, O2, and O3 in the anodic wave. However, the more negative values than the literature data for the formal potential of reactions including Nb(II)/Nb and Nb(III)/Nb are possibly due to the relatively lower concentrations of Nb(III) and Nb(II) compared to other experiments performed in the literature, where those ions were directly introduced to an electrolyte by the dissolution of Nb metal. The calculated formal potential with acceptable uncertainty ranges indicates that the redox reactions to be coupled are reliably hypothesized.

4.3. XRD analysis

It was reported by Arurault et al. [19] and Stöhr et al. [24] that a melt containing Nb(V) completely reacted to produce Nb(IV) due to an 'auto-reduction' process without any additional reductants as follows:



The possibility of the consumption of Nb(V) ions by the chemical reaction of Eq. (17) was previously investigated by Arurault et al. who observed the evolution of chlorine gas and an XRD analysis of frozen electrolytes [19]. They reported that Nb(V) was reduced to Nb(IV) by the chlorine ion when NbCl₅ was used as the solute.

Since the auto-reduction process reported in the literature can affect the quantity of Nb ions with different oxidation states depending on dissolution time of the NbCl₅ into LiCl–KCl, it is necessary to estimate the oxidation states of Nb ion in the ternary salts.

In this study, the XRD pattern (Bruker-AXS D8) was analyzed for the frozen salt obtained at a different time after the cell containing LiCl–KCl–NbCl₅ mixture was installed into the furnace. XRD measurement was performed at room temperature using Cu–K(α) radiation (wavelength = 1.5406 Å) generated by striking the electrons of 4 kV voltage. The XRD profile of each sample was recorded over 2θ from 20° to 80° in $\theta/2\theta$ step-scan mode with a scan time of 10 s per 0.02° step. The measured XRD profiles were analyzed using JADE 9 software which is a powder diffraction analysis package.

The XRD patterns found that Nb ion was present as Nb(V) in LiCl–KCl–NbCl₅ mixture as shown in Fig. 11. The peak intensities for crystals containing Nb were very weak due to the low concentration of Nb in the salt mixture, but several compounds were detected, including KNbCl₆, KNbO₃, LiNb₃O₈, and Nb₂O₅. The formation of Nb oxide compounds is inevitable due to the high oxygen affinity of Nb during the sample preparation in an air atmosphere. It should be noted that the oxidation state of Nb is Nb(V) in all the identified compounds. The auto-reduction reaction of NbCl₅ into NbCl₄ was expected to be unspontaneous based on the change in the Gibbs free energy of the reaction (summarized in Table 6), which was calculated by using data reported by Brocchi [34]. Also, although Nb chloride compounds reacted with oxygen, the oxidation state of Nb did not alter.

It is known that the oxygen ion decreases the oxidizing power of Nb(V) [26], which in turn increases the stability of Nb(V) not to react. Also, since the Nb oxychloride complexes, such as NbOCl_5^{2-} , are known to be more stable than the pure chloride complex of NbCl₆⁻, the oxidation state of Nb is dominantly Nb(V) once the oxygen is introduced into the cell. The more stable Nb oxychloride might cause Nb(III) to be reduced into the metallic Nb at more negative potentials as found in this study, which is consistent with results by Chemla et al. [35].

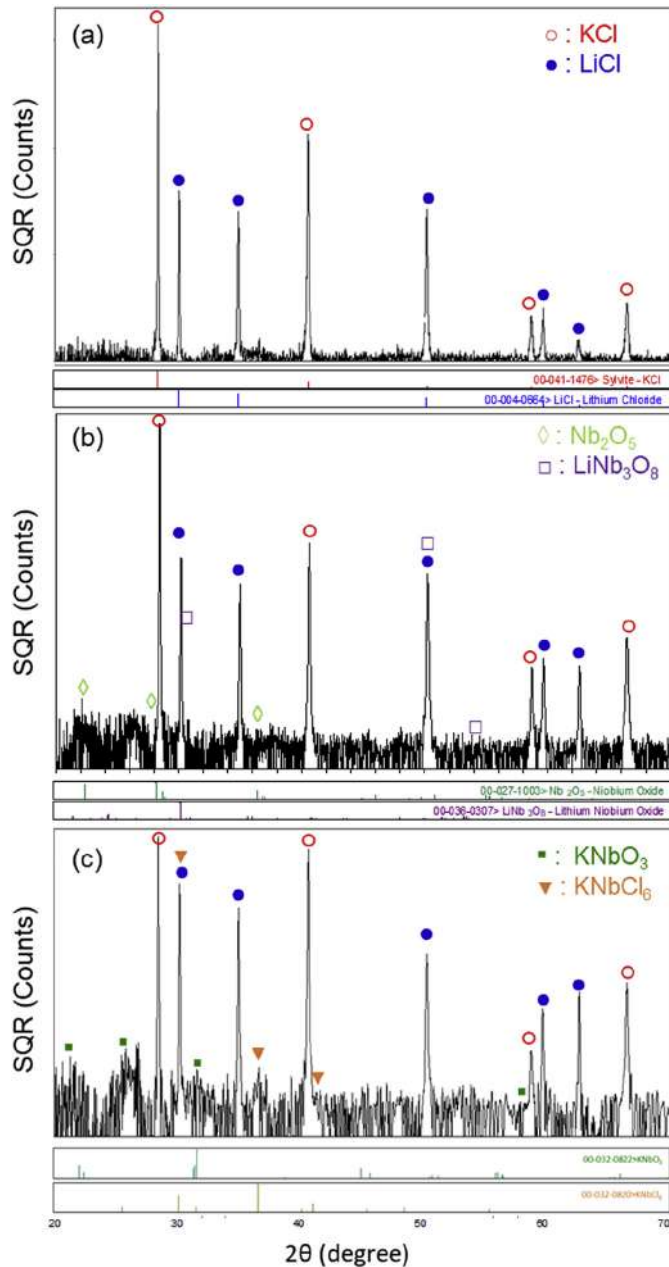


Fig. 11. X-ray diffraction patterns for the salt mixture of (a) pure LiCl–KCl, and LiCl–KCl–NbCl₅ obtained at the different time; (b) right after being inserted to the furnace, and (c) 24 h later after being melted.

The auto-reduction of Nb(V) into Nb(IV) with the evolution of chlorine gas was also reported by Lorthioir et al. [36] and Brevnova et al. [37]. Based on their results, it appears that the thermal stability of NbCl₅ decreases as the concentration of Nb and temperature increase. However, it is difficult to examine the effect of this reaction on experiments in this study due to the fact that; 1) no any compounds related to Nb(IV) were found by comparing the XRD profiles from the frozen LiCl–KCl–NbCl₅ obtained at the beginning of the melting (Fig. 11(b)) as well as 24 h later after the melting (Fig. 11(c)), 2) the Nb concentration (0.34 wt%) was much lower than that (>3.0 wt%) in the other experiment [37], 3) the operating temperature was 450 °C with LiCl–KCl eutectic salt in this study while, in the literature, self-reduction was observed at temperatures higher than 750 °C with NaCl–KCl eutectic salt [19,24].

It has also been reported that silica (SiO₂) used for a reference

Table 6

Changes of Gibbs free energy of reactions related to the Nb chloride and oxychloride.

Reaction	Gibbs free energy of reaction (ΔG) at different temperature (°C) (kJ/mol)			
	T = 100	T = 200	T = 300	T = 450
$\text{NbCl}_5 \rightarrow \text{NbCl}_3 + \text{Cl}_2$	168.9	156.9	160.3	171.0
$\text{NbCl}_5 \rightarrow \text{NbCl}_4 + \frac{1}{2}\text{Cl}_2$	84.3	79.4	89.4	111.4
$\text{NbCl}_5 + \frac{5}{4}\text{O}_2 \rightarrow \frac{1}{2}\text{Nb}_2\text{O}_5 + \frac{5}{2}\text{Cl}_2$	-197.8	-209.0	-205.2	-194.6
$\text{NbCl}_5 + \frac{1}{2}\text{O}_2 \rightarrow \text{NbOCl}_3(\text{s}) + 2\text{Cl}_2$	-54.1	-73.6	-78.7	-74.6
$\text{NbCl}_5 + \frac{1}{2}\text{O}_2 \rightarrow \text{NbOCl}_2 + \frac{3}{2}\text{Cl}_2$	-15.4	-20.7	-21.2	-4.4
$\text{NbCl}_4 + \frac{5}{4}\text{O}_2 \rightarrow \frac{1}{2}\text{Nb}_2\text{O}_5 + 2\text{Cl}_2$	-281.1	-285.9	-296.1	-305.1

electrode or a cell crucible reacted with NbCl₅, yielding Nb oxychloride and SiCl₄ formation [28]. However, no compounds containing Si element were found in XRD profiles in this study. No additional evidence of either corrosion on the reference electrode or wall of the cell, or the formation of Si-included compounds was found during the CV conducted in this study.

4.4. Suggestions for the electrorefining of Nb-containing waste

Radioactive wastes containing Nb can be categorized into three major groups; Zr-based alloy (Zr–Nb), steel (Fe–Cr–Nb), and Ni-based alloy (Ni–Cr–Nb). If these alloys are irradiated for several decades inside a nuclear reactor, they could be classified as intermediate level radioactive wastes because of Nb-94, while other elements would have radioactivity leading to classification as very low-level or low-level radioactive wastes. It is known that the standard electrode potential (E_0 vs. Cl₂/Cl⁻) of those major elements can be arranged in order of increasing electrochemical nobility as: Zr (-2.186 V) < Cr (-1.641 V) < Nb (-1.472 V) < Fe (-1.388 V) < Ni (-1.011 V) < Mo (-0.854 V) [38,39]. Depending on the composition of irradiated alloys, different processes to decontaminate Nb via electrorefining has been proposed as summarized in Fig. 12. Details are described as follows:

- 1) Zr–Nb: Nb is the alloying element in Zr-based alloys with content ranging from 1.0 to 2.5 wt%. Since Zr has a greater oxidation tendency than Nb, Zr can be separated from the alloys without the anodic dissolution of Nb by the anode potential control [40]. Since the residual at the anode containing most of the Nb is disposed of as intermediate level waste, the dissolution of Nb during electrorefining should be minimized by the potentiometric control to avoid salt contamination.
- 2) Fe-based alloy: Stainless steels including type 316, and 347 used in the reactor structural component contain less than 0.5 wt% Nb as a minor alloying element. Cr, the major alloying element with content of 9–12 wt%, is the noblest element among the alloying elements. In steels, Cr and Nb are fully soluble in the Fe matrix within their general concentrations. Thus, for the recovery of Fe and Cr via electrorefining in the presence of Fe(II), the dissolution of Cr occurs which is followed by that of Nb from the anode while the metallic Fe is deposited at the cathode. The recovered Fe alloy after the extraction of Nb can be regarded as low-level waste.

After electrorefining, the sequential electrolysis is required to purify the residual molten salt by extracting Nb for the disposal and Cr for the recycling. It should be noted that the equilibrium potentials for Nb(III)/Nb and Cr(III)/Cr are expected to depend on ion concentrations, which can be represented by the Nernst equation

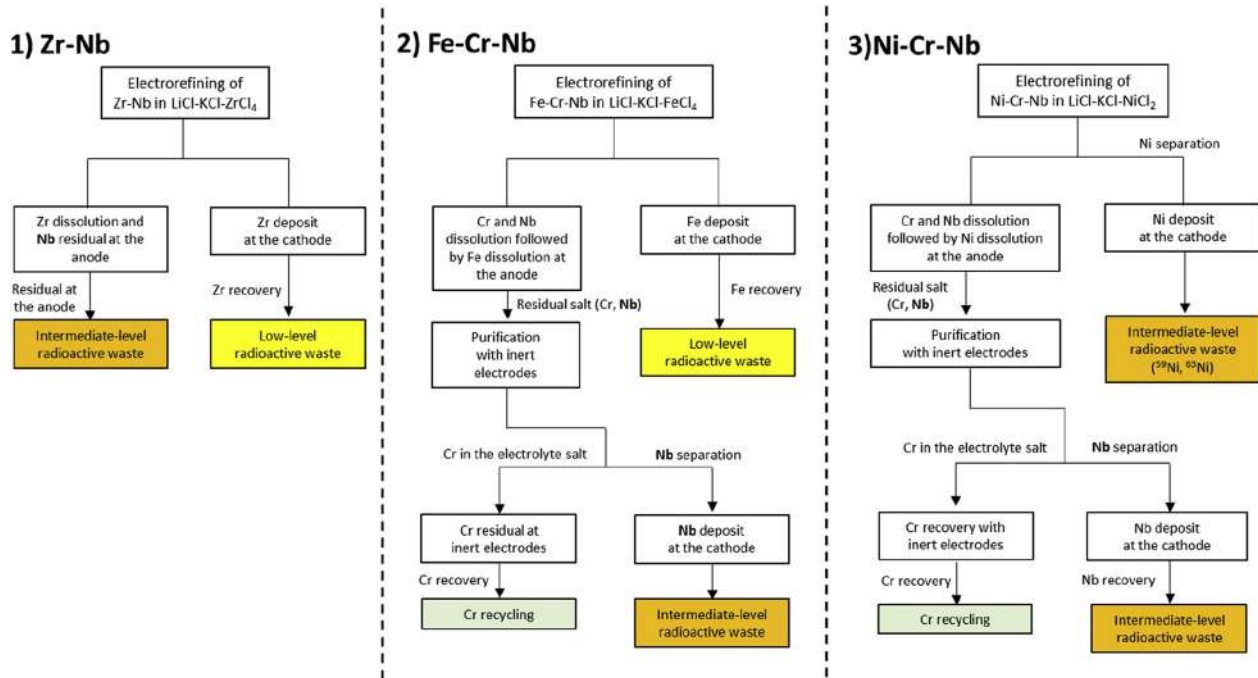


Fig. 12. Flowcharts for electrolytic refining processes for different radioactive wastes containing Nb.

as follows:

$$E_{\text{eq}} = E^0 - \frac{RT}{nF} \ln \frac{1}{\gamma_{\text{ox}} C_{\text{ox}}} \quad (18)$$

where E_{eq} is the equilibrium potential, T is the temperature in K, n is the number of transferred electrons, γ is the activity coefficient, and C is the concentration in $\text{mol} \cdot \text{cm}^{-3}$ where the subscript stands for the oxidized species. It is assumed that the activity coefficient for the oxidized species is the unity used to calculate E_{eq} by Eq. (18) for Nb(III)/Nb and Cr(III)/Cr as shown in Fig. 13(a). As a result, it is found that Nb can be separated without Cr co-deposition due to its more positive equilibrium potential than Cr, even taking into account the ~22 times higher concentration of Cr than that of Nb.

When Nb ions are reduced to metallic Nb in the residual molten salt by the additional electrodeposition process, the deposited Nb can be dissolved by the disproportionation reaction in the presence of Nb(V) as an initiator of electrorefining, which is described as follows:



Thus, it might be useful for more efficient Nb separation to introduce a high concentration of Nb(IV) to suppress the disproportionation reaction that causes the re-dissolution of the deposited Nb at the cathode.

3) Ni-based alloy: Ni-based alloys, including Inconel 625 (Ni–22Cr–9Mo–3.5Nb) and 718 (Ni–19Cr–5.2Nb), are widely used as structural materials in the part-strength control rod and the holddown spring in the fuel rod respectively. By the same principle described for Fe-based alloy wastes, it is possible to extract Ni at the first electrolytic refining process since Ni is much nobler than Cr and Nb. Then, Nb can be separated from the residual salt due to the fact it is nobler than Cr, as can be noticed in Fig. 13(b) for E_{eq} while the Cr remained in the residual salt, which can be recycled by another process for Cr recovery.

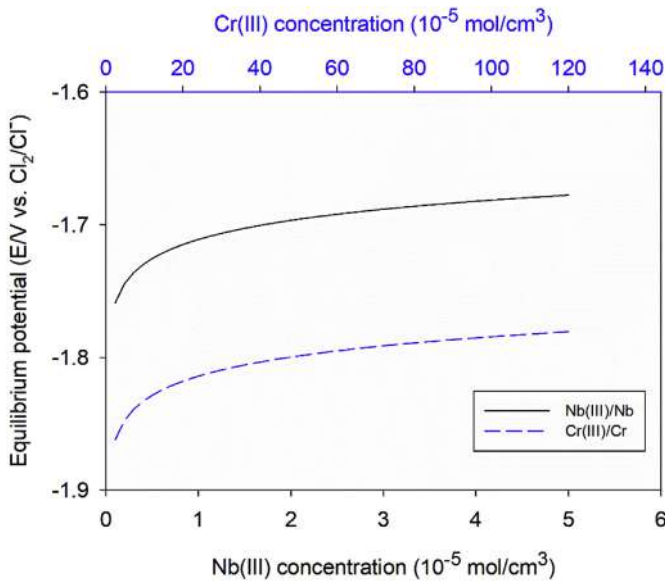
As discussed earlier, the deposition of insoluble Nb subchloride compounds can occur prior to that of metallic Nb since those chloride compounds are deposited at a more positive potential than the reduction potential of Nb ions. However, as mentioned, when a potential which is more negative than -0.6 V (vs. Ag/AgCl) is applied, only metallic Nb is deposited via the two-step reaction via the formation of Nb(II) on the electrode surface, as can be seen from the CV results. The transition in the composition of the deposit from Nb subchloride to metallic Nb was consistent with the XRD results reported by Lantelme et al. [26]. Thus, the sufficiently negative potential should be applied at the cathode to reduce Nb ions to metallic Nb during the decontamination process.

The concentration of Nb ions and their oxidation state are critical factors during electrorefining for the field of radioactive waste management to enhance the separation efficiency of Nb. It might be effective to use a low concentration of NbCl₅ in terms of the recovery of Nb in the metallic form due to the fact that 1) the possibility of the auto-reduction process decreases, and 2) the disproportionation reaction between metallic Nb and Nb(V) is suppressed as less Nb(V) is available. Maintaining a lower concentration of Nb can also prevent co-deposition by suppressing the existence of subchlorides.

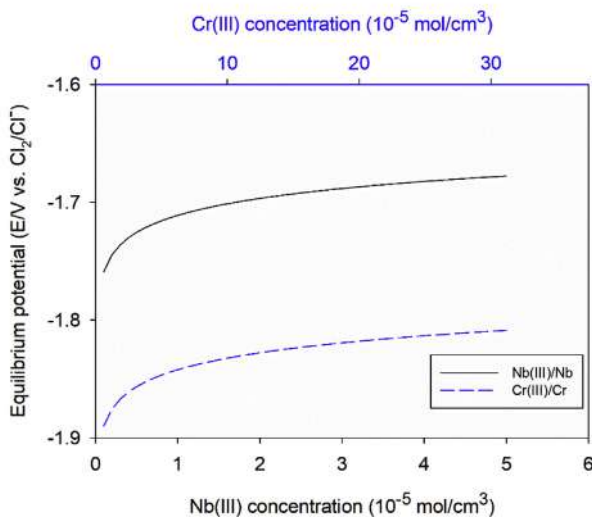
Moreover, it is suggested additives, such as heavy alkali metal chlorides or alkali fluorides which stabilize Nb(IV) and reduce the oxidizing power of Nb(V) as reported by Rosenkilde et al. [23] and Lantelme et al. [26], can be utilized to improve the deposition of metallic Nb. Further studies will be required to optimize the concentration of Nb ions with additives during the electrochemical process in order to achieve more efficient Nb extraction.

5. Conclusions

The electrochemical behaviors of Nb were examined in LiCl–KCl–NbCl₅ molten salt with 1.0 wt% NbCl₅ via several electrochemical techniques including chronoamperometry and cyclic voltammetry. All the experiments were performed within a well-controlled inert environment to minimize any experimental



(a) Cr/Nb concentration ratio = 22



(b) Cr/Nb concentration ratio = 6.3

Fig. 13. Comparison of equilibrium potentials depending on the concentration of Nb(III) and Cr(III) at 450 °C in the residual salt after electrolytic refining processing for wastes of (a) Fe-based alloy and (b) Ni-based alloy (Standard electrode potentials from Ref. [38]).

uncertainties.

The colors of the solution containing the different oxidation states of Nb ions were examined. They were compared to the relevant data from the existing literature, which confirmed that the color of the solution changed from pale-gray to yellow-orange when the oxidation state of Nb increased from +3 to +5.

Four and five different reduction and oxidation peaks were found by multiple sets of cyclic voltammetry with different scan range at the selected scan rates in order to identify the possible reduction and oxidation reactions at each peak potential, and to examine the reversibility of the corresponding reaction. It was found that the redox couples including Nb(V)/Nb(IV) and Nb(IV)/Nb(III) were reversible, as reported in the literature. The reliability

of experiments was confirmed by comparing the obtained data for the diffusion coefficient of Nb(V) and (IV) with the available literature data. This comparison also implies that 1) the diffusion coefficient of Nb(V) is the lowest among the stable Nb ions in LiCl–KCl at 450 °C, and 2) the diffusion coefficient of Nb(III) is possibly lower than that of Nb(IV). The negative and positive potential shifts were found for the other cathodic and anodic peaks respectively, which indicated that reactions involved in those peaks are irreversible.

Three additional redox couples were hypothetically proposed; Nb(III)/NbCl_x (2.33 < x < 3.13), Nb(III)/Nb and Nb(II)/Nb. The formal potentials of each redox couple were calculated using experimental data of the peak-to-peak separation from the voltammograms, and they were compared to the literature data in the LiCl–KCl system at 450 °C. A slight overprediction was found for those couples, but it was in good agreement within the acceptable range of ±0.1 V. The deposition of the metallic Nb became more dominant than that of insoluble Nb chloride compounds when the applied potential became more negative than –0.7 V (vs. Ag/AgCl). Further study might be necessary to identify the exact reduction and oxidation behaviors related to the formation of those Nb subchlorides which competed in the deposition of the metallic Nb, and the effect of the concentration, as well as operating temperature, should be examined for a more efficient and effective reduction process of metallic Nb.

The possibility of the auto-reduction process between Nb(V) and Nb(IV) was examined using X-ray diffractometry for the powder of LiCl–KCl–NbCl₅ mixtures which were obtained at different exposure times at 450 °C after melting. Several Nb compounds with pentavalent states were detected although the peak intensities of compounds that contained Nb were very weak. Thus, the effect of the auto-reduction reaction on the initial concentration of Nb(V) in the cell was negligible.

Different schemes for the electrolytic refining of Nb-containing radioactive wastes, including Zr–Nb, Fe and Ni alloys, were clarified with consideration for the standard electrode potentials of major elements of concern for radioactivity management. Depending on their order of reduction potentials, it is expected that Nb can be extracted from the anode or molten electrolyte remaining after the main electrolytic refining process to recover base metal elements including Zr, Fe, or Ni. This Nb separation process is important in terms of recycling the salt electrolyte and reducing the volume and radioactivity of wastes. For more efficient Nb extraction, it is necessary to optimize the concentration of Nb ions in the salt electrolyte and to apply a more negative potential to the cathode to promote the deposition of metallic Nb without the formation of insoluble Nb chloride compounds.

Acknowledgments

This work was supported by the National Research Foundation of Korea grant funded by the Korea government (MSIT) (No. 2019M2A7A1001758).

References

- [1] Nuclear Data Center at Korea Atomic Energy Research Institute, Table of nuclides, Available on the Internet at, <http://atom.kaeri.re.kr:8080/ton/index.html>, 2000.
- [2] R. Granier, D. Gambini, *Applied Radiobiology and Radiation Protection*, Ellis Horwood, 1990, pp. 346–347.
- [3] K. Noh, C.J. Hah, Verification of MCNP/ORIGEN-2 model and preliminary radiation source term evaluation of wolsung unit 1, *J. Nucl. Fuel Cycle and Waste Technol.* 13 (1) (2015) 21.
- [4] D.-K. Cho, G. Sun, J. Choi, D. Hwang, H.-S. Kim, T.-W. Hwang, Verification of source term analysis system for decommissioning wastes from a CANDU reactor, in: *Proceedings of the ASME 13th International Conference on Environmental Remediation and Radioactive Waste Management (ICEM)*, 3–7 October 2010, Tsukuba, Japan.

- [5] Jaeyoung Park, Sungyeol Choi, Sungjune Sohn, Il Soon Hwang, Cyclic voltammetry on Zr, Sn, Fe, Cr and Co in LiCl-KCl salts at 500 °C for electrorefining of irradiated Zircaloy-4 cladding electrochemical/electroless deposition, *J. Electrochem. Soc.* 164 (12) (2017) D744–D751.
- [6] Jaeyoung Park, Sungyeol Choi, Sungjune Sohn, K.-R. Kim, Il Soon Hwang, Cyclic voltammetry on zirconium redox reactions in LiCl-KCl-ZrCl₄ at 500 °C for electrorefining contaminated Zircaloy-4 cladding, *J. Electrochem. Soc.* 161 (3) (2014) H97–H104.
- [7] K.H. Lim, J.-I. Yun, Study on the exchange current density of lanthanide chlorides in LiCl-KCl molten salt, *J. Nucl. Mater.* 295 (1) (2019) 577.
- [8] D. Rappleye, M.L. Newton, C. Zhang, M.F. Simpson, Electroanalytical measurements of binary-analyte mixtures in molten LiCl-KCl eutectic: uranium (III)- and Magnesium (II)-Chloride, *J. Nucl. Mater.* 486 (1) (2017) 369.
- [9] C.K. Gupta, Extractive metallurgy of niobium, tantalum, and vanadium, *Int. Met. Rev.* 29 (1984) 4053.
- [10] D.R. Sadoway, Electrochemical processing of refractory metals, *J. Mater.* 43 (1991) 15.
- [11] Q. Zhiyu, T. Pierre, Electrochemical reduction of niobium ions in molten LiF-NaF, *J. Appl. Electrochem.* 15 (1985) 259.
- [12] F. Lantelme, Y. Berghoute, J.H. von Barner, G.S. Picard, The Influence of oxide on the electrochemical processes in K₂NbF₇-NaCl-KCl melts, *J. Electrochem. Soc.* 102 (1995) 4097.
- [13] V. Van, A. Silný, J. Hveš, V. Daněk, Electrochemical study of niobium fluoride and oxyfluoride complexes in molten LiF-KF-K₂NbF₇ bath, *Electrochem. Commun.* 1 (7) (1999) 295.
- [14] D.A. Vetrova, A.V. Popova, S.A. Kuznetsov, Electrochemical behavior of niobium complexes in chloride-fluoride melts with addition of alkaline cations, *ECS Trans.* 86 (14) (2018) 69.
- [15] A. Khalidi, P. Taxil, B. Lafage, A.P. Lamaze, Electrochemical reduction of niobium ions in molten NaCl-KCl, *Mater. Sci. Forum* 73–75 (1991) 421.
- [16] A. Barhoun, Y. Berghoute, F. Lantelme, Electrodeposition of niobium from fluoroniobate K₂NbF₇ solutions in fused NaCl-KCl, *J. Alloy. Comp.* 179 (1992) 241.
- [17] F. Lantelme, Y. Berghoute, Transient electrochemical techniques for studying electrodeposition of niobium in fused NaCl-KCl, *J. Electrochem. Soc.* 141 (1994) 3306.
- [18] F. Lantelme, Y. Berghoute, A. Salmi, Cyclic voltammetry at a metallic electrode: application to the reduction of nickel, tantalum and niobium salts in fused electrolytes, *J. Appl. Electrochem.* 24 (1994) 361.
- [19] L. Arurault, J. Bouteillon, J.C. Poignet, Chemical stability of solutions of niobium V in molten NaCl-KCl at 750°C, *J. Electrochem. Soc.* 9 (1995) 16.
- [20] A. Salmi, Y. Berghoute, F. Lantelme, Modelling multistep electrochemical reactions in molten salt electrowinning of refractory metals, *Electrochim. Acta* 40 (1995) 403.
- [21] B. Gillesberg, J.H. von Barner, N.J. Bjerrum, F. Lantelme, Niobium plating processes in alkali chloride melts, *J. Appl. Electrochem.* 29 (1999) 939.
- [22] C. Rosenkilde, T. Østvold, Chemistry of NbCl in the CsCl-NaCl eutectic melt, *Acta Chem. Scand.* 48 (1994) 732.
- [23] C. Rosenkilde, T. Østvold, Chemistry of NbCl in the CsCl-NaCl eutectic melt, *Acta Chem. Scand.* 49 (1995) 85.
- [24] U. Stöhr, W. Freyland, Electrochemical impedance investigation of redox mechanism of refractory metal compounds in molten salt, *Electrochim. Acta* 44 (1999) 2199.
- [25] G.S. Picard, P. Bocage, Niobium chemistry in molten LiCl-KCl eutectic, *Proc. Electrochem. Soc.* 16 (1992) 622.
- [26] F. Lantelme, A. Barhoun, J. Chevalet, Electrochemical behavior of solutions of niobium chlorides in fused alkali chlorides, *J. Electrochem. Soc.* 31 (1993) 324.
- [27] M. Mohamedi, Y. Sato, T. Yamanura, Examination of niobium electrochemistry from the reduction of Nb₃Cl₈ in LiCl-KCl eutectic, *Electrochim. Acta* 44 (1994) 1559.
- [28] I. Elizarova, E. Polyakov, L. Polyakova, *Mater. Sci. Forum* 3 (1991) 393.
- [29] F. Lantelme, H. Groult, *Molten Salts Chemistry: from Lab to Applications*, Elsevier Science, 2013.
- [30] S.P. Fusselman, J.J. Roy, D.L. Grimmer, L.F. Grantham, C.L. Krueger, C.R. Nabelek, T.S. Storvick, T. Inoue, T. Hijikata, K. Kinoshita, Y. Sakamura, K. Uozumi, T. Kawai, N. Takahashi, Thermodynamic properties for rare earths and americium in pyropartitioning process solvents, *J. Electrochem. Soc.* 2573 (1999) 801.
- [31] A.J. Bard, L.R. Faulkner, *Electrochemical Methods: Fundamental and Applications*, second ed., John Wiley & Sons, Hoboken, NJ, 2001.
- [32] L. Yang, R.G. Hudson, *J. Electrochem. Soc.* 106 (1959) 986.
- [33] R.J. Klingler, J.K. Kochi, *J. Phys. Chem.* 85 (3) (1981) 1731.
- [34] E.de A. Brocchi, Reduction Chlorination Reactions of Niobium and Tantalum Oxide Containing Materials, Ph.D. Thesis, Imperial College of Science and Technology, London, 1983, pp. 37–44.
- [35] M. Chelma, V. Grinevitch, *Bull. Soc. Chim. France* 3 (1973) 853.
- [36] G. Lorthioir, A. Saile, F. Basile, *Fr. Mater. Sci. Forum* 449 (1991) 73–75.
- [37] N.P. Brevnova, I.B. Polovov, M.V. Chernyshov, V.A. Volkovich, B.D. Vasin, T.R. Griffiths, Electronic absorption spectra of niobium species in halide melts, *ECS Trans.* 50 (1) (2012) 325.
- [38] M. Iizuka, T. Inoue, O. Shirai, T. Iwai, Y. Arai, Application of normal pulse voltammetry to on-line monitoring of actinide concentrations in molten salt electrolyte, *J. Nucl. Mater.* 297 (2001) 43.
- [39] H.C. Gaur, H.L. Jindal, Standard electrode potentials in molten chlorides, *Electrochim. Acta* 13 (4) (1968) 835.
- [40] Sungjune Sohn, Jaeyoung Park, Il Soon Hwang, Electrolytic recovery of high purity Zr from radioactively contaminated Zr alloys in chloride salts, *Int. J. Electrochem. Sci.* 13 (2018) 3897.

Nomenclature

- CA: Chronoamperometry
 CV: Cyclic voltammetry
 i_p : Current at the peak potential
 n : Number of the transferred electron involved in a reaction
 A : Surface area of the electrode
 C^0 : Bulk concentration of the species involved in the reaction
 F : Faraday constant
 D_0 : Diffusion coefficient of the species
 R : Gas constant
 T : Temperature
 v : Scan rate
 α : Charge transfer coefficient
 E_{pc} : Cathodic peak potential
 E_{pc} : Formal potential
 $D_{ox}D_{red}$: Diffusion coefficient of oxidized and reduced species
 E_{pa} : Anodic peak potential
 $E_{1/2}$: Half-wave potential
 k_s : Standard rate constant of the electrode reaction
 E_{eq} : Equilibrium potential
 γ_{ox} : Activity coefficient of the oxidized species